Osteoarthritis and Cartilage (2009) **17,** 64–72

doi:10.1016/j.joca.2008.05.020

Osteoarthritis and Cartilage

International Cartilage Repair Society

OARSI OSTEOARTHRITIS RESEARCH SOCIETY INTERNATIONAL

Inorganic pyrophosphate as a regulator of hydroxyapatite or calcium pyrophosphate dihydrate mineral deposition by matrix vesicles

C. Thouverey M.Sc.†‡§‖¶#, G. Bechkoff M.Sc.‡§‖¶#, S. Pikula Ph.D.† and R. Buchet Ph.D.‡§‖¶#*

† *Department of Biochemistry, Nencki Institute of Experimental Biology, Polish Academy of Sciences, PL-02093 Warsaw, Poland*

‡ *Université de Lyon, Lyon, F-69003, France*

§ *Université Lyon 1, Villeurbanne, F-69622, France*

‖ *INSA-Lyon, Villeurbanne, F-69622, France*

¶ *CPE Lyon, Villeurbanne, F-69616, France*

ICBMS CNRS UMR 5246, Villeurbanne, F-69622, France

Summary

Objective: Pathological mineralization is induced by unbalance between pro- and anti-mineralization factors. In calcifying osteoarthritic joints, articular chondrocytes undergo terminal differentiation similar to that in growth plate cartilage and release matrix vesicles (MVs) responsible for hydroxyapatite (HA) or calcium pyrophosphate dihydrate (CPPD) deposition. Inorganic pyrophosphate (PP_i) is a likely source of inorganic phosphate (P_i) to sustain HA formation when hydrolyzed but also a potent inhibitor preventing apatite mineral deposition and growth. Moreover, an excess of PP_i can lead to CPPD formation, a marker of pathological calcification in osteoarthritic joints. It was suggested that the P_i/PP_i ratio during biomineralization is a turning point between physiological and pathological mineralization. The aim of this work was to determine the conditions favoring either HA or CPPD formation initiated by MVs.

Methods: MVs were isolated from 17-day-old chicken embryo growth plate cartilages and subjected to mineralization in the presence of various P_i/PP_i ratios. The mineralization kinetics and the chemical composition of minerals were determined, respectively, by light scattering and infrared spectroscopy.

Results: The formation of HA is optimal when the P_i/PP_i molar ratio is above 140, but is completely inhibited when the ratio decreases below 70. The retardation of any mineral formation is maximal at P_i/PP_i ratio around 30. CPPD is exclusively produced by MVs when the ratio is below 6, but it is inhibited for the ratio exceeding 25.

Conclusions: Our findings are consistent with the P_i/PP_i ratio being a determinant factor leading to pathological mineralization or its inhibition.

Key words: Alkaline phosphatase, Calcium pyrophosphate dihydrate, Cartilage, Hydroxyapatite, Mineralization, Osteoarthritis, Pyrophosphate.

Abbreviations: AnxA2–A6 vertebrate annexin 2–6, AMP adenosine monophosphate, 5′AMPase 5′ adenosine monophosphatase, ATP adenosine triphosphate, ATPase adenosine triphosphatase, BCIP bromo-chloro-indolyl phosphate, bis-*p*-NPP bis-*p*-nitrophenyl phosphate, CPPD calcium pyrophosphate dihydrate, GPI glycosylphosphatidylinositol, HA hydroxyapatite, MVs matrix vesicles, NBT nitroblue tetrazolium, NPP1 nucleoside triphosphate pyrophosphatase phosphodiesterase 1, PAGE polyacrylamide gel electrophoresis, PDE phosphodiesterase, PI-PLC phosphatidylinositol specific phospholipase C, PME phosphomonoesterase, pMV pellet of MVs treated by PI-PLC, *p*-NPP *p*-nitrophenyl phosphate, P_i inorganic phosphate, PP_i inorganic pyrophosphate, SDS sodium dodecyl sulfate, SCL synthetic cartilage lymph, sMV supernatant of MVs treated by PI-PLC, TNAP tissue non-specific alkaline phosphatase.

Introduction

Physiological mineralization takes place during the formation and the development of mineralized tissues, e.g., bones and teeth[1–3]. In the prenatal and early postnatal life, biomineralization is the last essential event in the endochondral and intramembranous bone formation leading to the replacement of cartilaginous skeleton and craniofacial fibrous tissue by the definitive bone skeleton. Throughout life, the mineralization process continues to play a crucial role in bone remodeling and repair. The regulation of physiological mineralization is mediated at molecular, cellular and tissue levels[4] and involves coordination between stimulatory and inhibitory factors[3–6]. However, uncontrolled or pathological mineralization, due to an unbalance between pro- and anti-mineralization factors[3–6], can occur during aging, degenerative joint diseases, or genetic and various metabolic disorders. This causes an excessive mineral deposition in articular cartilages[7,8] that leads to joint inflammation and the progression of osteoarthritis. Several calcific diseases are characterized by the deposit of calcium pyrophosphate dihydrate (CPPD) or of hydroxyapatite (HA) in degenerative joints[3–10].

*Address correspondence and reprint requests to: Dr René Buchet, Ph.D., Université Lyon 1, Bâtiment Chevreul, 43 Boulevard du 11 Novembre 1918, F-69 622 Villeurbanne Cedex, France. Tel: 33-4-72-43-13-20; Fax: 33-4-72-43-15-43; E-mail: rbuchet@univ-lyon1.fr

Received 20 December 2007; revision accepted 23 May 2008.

During endochondral ossification, chondrocytes undergo a series of differentiation: cell proliferation, hypertrophy, terminal differentiation and cell apoptosis[11–14]. Hypertrophic chondrocytes initiate mineralization by releasing matrix vesicles (MVs)[14–16]. MVs are involved in the initial step of mineralization by promoting the formation of HA in their lumen[17]. Preformed HA is released from MV into the extracellular matrix, so that HA crystals continue to grow[6]. In contrast, chondrocytes in healthy articular cartilage maintain a stable phenotype[13] and their released MVs are unable to calcify[6]. These chondrocytes do not proliferate and produce extracellular matrix components such as chondroitin-4-sulfate, chondroitin-6-sulfate, keratansulfate, as well as types II, III, VI, IX and XI collagen[18].

Osteoarthritis is characterized by a degradation of the proteoglycan and collagen matrix[19] as well as by articular chondrocytes undergoing terminal differentiation similar to that in growth plate cartilage[3]. Osteoarthritic articular chondrocytes can release MVs[20–23], which are responsible for the initial formation of HA[20–23] or CPPD minerals[8,9,24,25] in degenerative joints. MVs from osteoarthritic cartilage own similar protein machinery than MVs from growth plate cartilage, necessary for Ca^{2+} uptakes into MV lumen: annexin A2 (AnxA2), AnxA5 and AnxA6[26], as well as for inorganic phosphate (P_i) homeostasis: tissue non-specific alkaline phosphatase (TNAP)[27,28], 5′ adenosine monophosphatase (5′AMPase)[28], ion-motive adenosine triphosphatase (ATPases)[28], and nucleotide pyrophosphatase/phosphodiesterase-1 (NPP1)[8,9,29]. In addition to these proteins, osteoarthritis articular chondrocytes express type X collagen (a marker of hypertrophic chondrocytes), osteonectin, bone morphogenetic proteins (which induce new bone formation) and RUNX2 (a transcription factor regulating hypertrophic chondrocyte differentiation)[26,30–32].

At enzymatic and molecular levels, NPP1 and TNAP have antagonistic effects[33–36] on mineral formation due to their opposing activities: production of Inorganic pyrophosphate (PP_i) by NPP1 or its hydrolysis by TNAP. TNAP provides P_i from various phosphate substrates during mineralization[37,38], whereas NPP1, and possibly TNAP[39], supplies PP_i from adenosine triphosphate (ATP) or uridine triphosphate (UTP) hydrolysis. At low concentrations, PP_i prevents the seeding of calcium phosphate minerals[40–44], while an excessive accumulation of PP_i in cartilage matrix leads to deposits of pathologic CPPD crystals, e.g., $Ca_2P_2O_7 \times 2\ H_2O$[45–47]. Ankylosis protein (ANK), a transmembrane protein that transports intracellular PP_i to the extracellular matrix[48–50], and NPP1, are overexpressed in chondrocytes of osteoarthritic articular cartilage, contributing to increase PP_i, where CPPD crystal formation could occur[29,51–53].

P_i/PP_i ratio could be a turning point to discern between physiological and pathological mineralization and therefore is subjected to tight regulation[37]. Since osteoarthritic MVs and growth plate MVs exhibit similar structural and functional properties, we selected MVs isolated from chick embryo growth plate cartilage to determine the effect of the P_i/PP_i ratio on HA and CPPD depositions.

Materials and methods

PURIFICATION OF MVs

MVs were isolated from growth plate and epiphyseal cartilage slices of 17-day-old chicken embryos by collagenase digestion[54], with slight modifications[55]. Seventeen-day-old chicken embryo leg bones were cut into 1–3-mm thick slices and washed five times in a synthetic cartilage lymph (SCL) containing 100 mM NaCl, 12.7 mM KCl, 0.57 mM $MgCl_2$, 1.83 mM $NaHCO_3$, 0.57 mM Na_2SO_4, 1.42 mM NaH_2PO_4, 5.55 mM D-glucose, 63.5 mM sucrose and 16.5 mM N-tris(hydroxymethyl)methyl 2-aminoethane sulfonic acid (TES) (pH 7.4). Growth plate and epiphyseal cartilage slices were digested at 37°C for 3.5–4 h in the SCL buffer with 1 mM Ca^{2+} and collagenase (500 units/g of tissue, type IA, Sigma). It was vortexed and filtered through a nylon membrane. The suspension was centrifuged at 600× *g* for 10 min to pellet intact hypertrophic chondrocytes. The supernatant was centrifuged at 13,000× *g* for 20 min. The pellet was discarded and the supernatant was submitted to a third centrifugation at 70,000× *g* for 1 h. The final pellet containing MVs was suspended in 300 μL of SCL buffer and stored at 4°C. The protein concentration in the MV fraction was determined using the Bradford assay kit (Bio-Rad). Proteins of MVs were separated in 7.5 or 10% (w/v) sodium dodecyl sulfate (SDS)-polyacrylamide gels[56]. The gels were stained with Coomassie Brilliant Blue R-250.

TRANSMISSION ELECTRON MICROSCOPY

A 20 μL aliquot of MV fraction was transferred to carbon-coated grids. The grids were negatively stained with 2% uranyl acetate and dried. The grids were viewed with an electron microscope Philips CM140 at 80 kV accelerating voltage.

TREATMENT OF MVs BY PHOSPHATIDYLINOSITOL SPECIFIC PHOSPHOLIPASE C

MVs (1 μg of MV proteins/μL) were incubated in SCL with 10 mM Mg^{2+}, 5 μM Zn^{2+} and 1 unit of phosphatidylinositol specific phospholipase C (PI-PLC) per mL for 7 h at 37°C under gentle agitation. The supernatant of MVs (sMVs) treated by PI-PLC containing MV glycosylphosphatidylinositol (GPI)-anchored proteins and the pellet (pMV) were separated by centrifugation at 90,000× *g* for 30 min. The pellet of MVs treated by PI-PLC (pMV) was resuspended in the same volume of SCL as before the centrifugation.

IMMUNODETECTION OF CHICKEN CAVEOLIN-1

Proteins of MVs were separated in 12% (w/v) SDS-polyacrylamide gels[56] and then electro-transferred (Mini-ProteanII™ Kit, Bio-Rad) onto nitrocellulose membranes (Hybond™–ECL™, Amersham Biosciences)[57]. The nitrocellulose membranes were blocked with 5% (w/v) milk in a buffer (20 mM Tris–HCl, pH 7.5, 150 mM NaCl) for 1 h at room temperature, then incubated with 3% (w/v) milk and 0.1% (v/v) mouse monoclonal IgG against chicken caveolin-1 (BD Biosciences) in tween 20 tris buffered saline (TTBS) buffer (20 mM Tris–HCl, pH 7.5, 150 mM NaCl, 0.05% (v/v) Tween 20) at 4°C overnight. The nitrocellulose membranes were washed several times with TTBS and incubated with 3% (w/v) milk and 0.05% (v/v) goat anti-mouse IgG conjugated with alkaline phosphatase (Immuno-Blot Assay Kit, Bio-Rad) in TTBS buffer. The membranes were washed, and bands were visualized by addition of color-developing solution according to the manufacturer's instructions.

SPECIFIC REVELATION OF ALKALINE PHOSPHATASE

MV proteins were incubated under mild denaturing conditions (without heating before the gel migration) in the Tris buffer containing 2% SDS but no β-mercaptoethanol to preserve the TNAP activity. After the migration, SDS-polyacrylamide gels were incubated in a solution containing 0.1 M Tris–HCl (pH 9.6), 0.1 M NaCl, 5 mM $MgCl_2$, 0.24 mM bromo-chloro-indolyl phosphate (BCIP), a TNAP substrate and 0.25 mM nitroblue tetrazolium (NBT) until the blue band associated to alkaline phosphatase was visible[39].

ENZYMATIC ASSAYS

The phosphomonoesterase (PME) activity was measured at pH 7.4 or 10.4, using 10 mM *p*-nitrophenyl phosphate (*p*-NPP) as a substrate[58], in 25 mM piperazine and 25 mM glycylglycine buffer, by monitoring the release of *p*-nitrophenolate at 420 nm ($\varepsilon = 9.2\ cm^{-1}\ mM^{-1}$ at pH 7.4; $\varepsilon = 18.5\ cm^{-1}\ mM^{-1}$ at pH 10.4, M^{-1}). One unit of PME activity corresponds to the amount of enzyme hydrolyzing 1 μmol of *p*-NPP per minute at 37°C. The phosphodiesterase (PDE) activity of MVs was measured at pH 7.4 or at 9, with 2 mM bis-*p*-nitrophenyl phosphate (bis-*p*-NPP) as substrate in 25 mM piperazine and 25 mM glycylglycine buffer, and monitoring the release of *p*-nitrophenolate at 420 nm ($\varepsilon = 9.2\ cm^{-1}\ mM^{-1}$ at pH 7.4; $\varepsilon = 17.8\ cm^{-1}\ mM^{-1}$ at pH 9)[39]. One unit of PDE activity corresponds to the amount of enzymes hydrolyzing 1 μmol of bis-*p*-NPP per minute at 37°C. To determine the pyrophosphatase activity, MVs were incubated in 25 mM piperazine and 25 mM glycylglycine buffer (at the indicated pH) containing 0.25–2 mM PP_i, for 20 min at 37°C. The reaction was stopped by adding 10 mM levamisole and stored at 4°C. Aliquots of the reaction mixture were collected to determine PP_i concentrations with the Sigma reagent kit. One unit of pyrophosphatase activity corresponds to the amount of enzymes hydrolyzing 1 μmol of PP_i per minute at 37°C.

DETERMINATION OF MINERALIZATION KINETICS

Aliquots of the MV stock solution were diluted to a final concentration of 20 μg of MV proteins/mL in the SCL buffer containing 2 mM Ca^{2+} and different concentrations of ions (P_i, PP_i) or phosphate substrates [adenosine monophosphate (AMP), ATP], as indicated in the figure legends. They were incubated at 37°C and their absorbances at 340 nm were measured at 15-min intervals with Uvikon spectrophotometer model 932 (Kontron Instruments). When MVs were incubated in SCL containing 2 mM Ca^{2+} but not P_i, PP_i and other phosphate substrates, there were no changes in turbidity. Thus, the increase in turbidity was due to mineral formation[59,60].

IDENTIFICATION OF MINERALS BY INFRARED SPECTROSCOPY

The minerals were determined by infrared spectroscopy (Nicolet 510M FTIR spectrometer). They were centrifuged at 3,000× *g* for 10 min and washed several times with water. They were dried and incorporated by pressing into 100 mg of KBr. Standard CPPD was prepared by incubating stoichiometric proportions of Ca^{2+} and PP_i at 37°C for 2 weeks. Standard HA was purchased from Sigma.

Results

BIOCHEMICAL CHARACTERIZATION OF MVs

The MVs extracted from chicken embryo growth plate cartilages were round structures with a diameter ranging from 100 to 250 nm (Fig. 1), in agreement with Anderson *et al.*[61] and Balcerzak *et al.*[55]. The electrophoresis profile of MVs exhibited, among others, three major bands with apparent molecular weights of 44, 38 and 31 kDa [Fig. 2(A)][59]. Caveolin-1, a marker of caveolae, present in the plasma membrane of hypertrophic chondrocytes [26 kDa, Fig. 2(B), lane 2], was absent in MVs [Fig. 2(B), lane 1], indicating that isolated MVs are not contaminated by the fragments of plasma membrane. TNAP, a marker enzyme of MVs[62], involved in the P_i homeostasis in mineralizing tissues[63–65], was enriched in the MV fractions. The PME activity associated with TNAP of MVs at pH 10.4 was 25.0 ± 3.4 units/mg of proteins, approximately five times higher in comparison to hypertrophic chondrocytes (Table I), indicating a high degree of purity of MV preparations.

EXTRAVESICULAR P_i AND PP_i HOMEOSTASIS BY MVs

To delineate the importance of TNAP in PME and pyrophosphatase activities of MVs, the enzyme was digested out from MVs by a cleavage of its GPI anchor with PI-PLC. GPI-anchored TNAP in untreated MVs exhibited an apparent molecular weight of 118 kDa (Fig. 3, lane 1). After centrifugation, TNAP without GPI anchor was detected in the supernatant (sMV, Fig. 3, lane 2), but not in the pellet

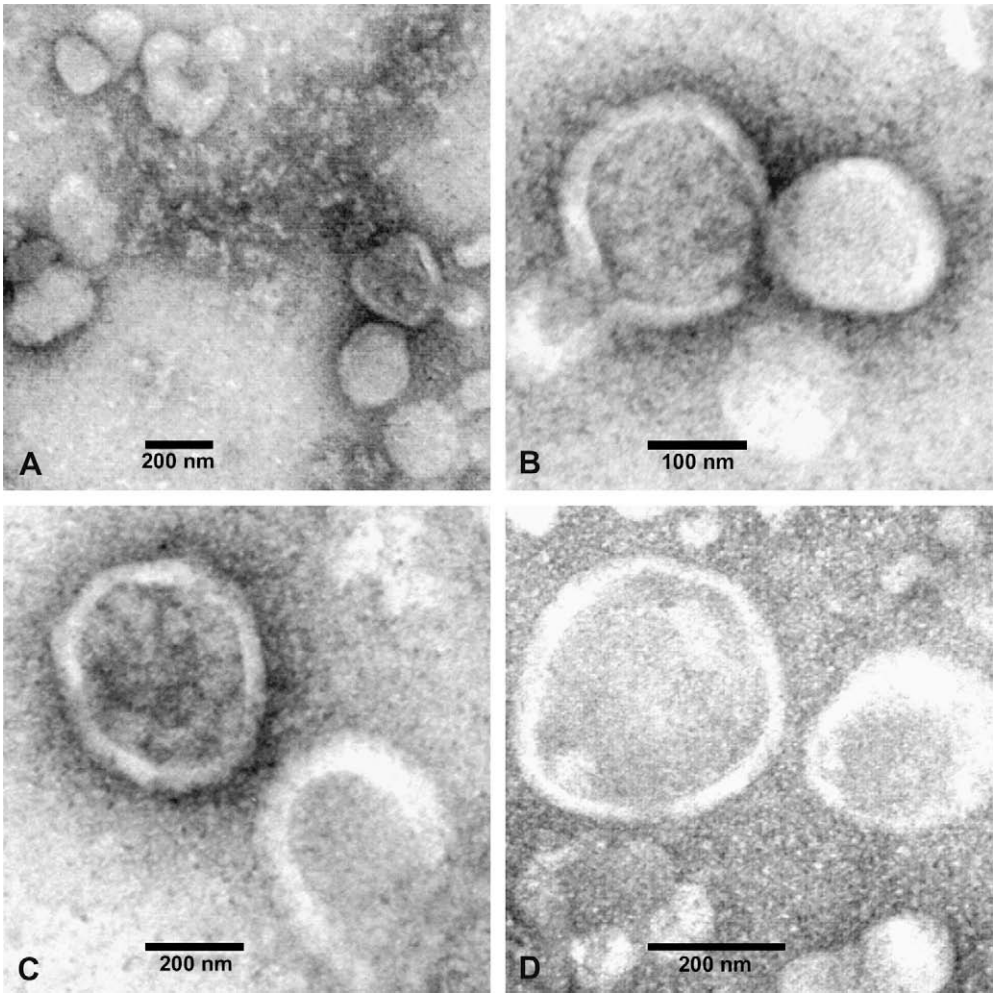

Fig. 1. Electron microscope view of MVs. MVs exhibit spherical shapes with a 100–250 nm diameter (magnifications: A, ×53,000; B, ×100,000; C, ×75,000; D, ×100,000).

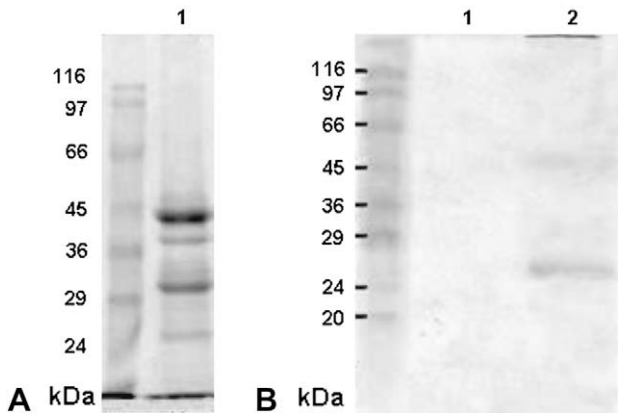

Fig. 2. (A) Protein pattern of MVs in a 10% SDS-polyacrylamide gel. Lane 1, MVs. (B) Western-Blot of MVs and hypertrophic chondrocytes for the detection of caveolin-1. Lane 1, MVs; Lane 2, co-isolated chondrocytes.

containing MVs devoid of GPI-anchored proteins (pMV, Fig. 3, lane 3). The specific PME activity of MVs amounted to 0.62 ± 0.10 units/mg of MV proteins at physiological pH, e.g., 40 times lower than at pH 10.4 (Table II). The percentage of total PME activity of the sMV was $92 \pm 3.7\%$ at pH 10.4 and $91 \pm 3\%$ at pH 7.4 (Table II), indicating that more than 91% of PME activity is associated with TNAP in MVs. The PDE activity of MVs reflecting both TNAP[39] and NPP1 activities[35] was 2.66 ± 0.30 units/mg of MV proteins at optimal conditions (pH 9). It was 0.52 ± 0.08 units/mg of MV proteins at pH 7.4. When the substrate concentration was reduced from 2 to 0.5 mM, the optimal pH for the activity shifted from 8.8 to 8.2 (Fig. 4). In the presence of 2 mM PP_i, the pyrophosphatase activity of MVs was 3.70 ± 0.31 units/mg of MV proteins at pH 8.8, and 1.00 ± 0.08 units/mg of MV proteins at physiological pH (Table II). The apparent K_m of PP_i hydrolysis at physiological pH was identical for MVs, sMV and pMV, and amounted to 355 ± 6 μM. The pyrophosphatase activity of all these samples was also inhibited in the same competitive manner by P_i; K_i amounted to 3.63 ± 0.14 mM. Over $96 \pm 5.2\%$ of the pyrophosphatase activity was attributed to the sMV at pH 7.4 (Table II), indicating that the ability of MVs to hydrolyze PP_i was due to TNAP.

P_i AND NUCLEOTIDE-INITIATED MINERALIZATION BY MVs

The isolated MVs, incubated in the SCL buffer with 2 mM Ca^{2+} were able to induce mineral formation, after a short lag period of 3.5–4 h, corresponding to the time of accumulation of Ca^{2+} and P_i within MVs[60]. Then, the mineral formation increased rapidly and reached saturation (Fig. 5). MVs in SCL medium without Ca^{2+} were not able to mineralize, indicating that the presence of 0.57 mM Mg^{2+} in SCL medium containing MVs cannot induce mineral formation. No mineral was formed in the SCL buffer with 2 mM Ca^{2+} devoid of MVs, indicating that MVs are essential to initiate mineralization.

The MV-induced mineral was identified by infrared spectroscopy. The infrared spectrum of mineral formed by MVs in SCL buffer exhibited five peaks at 1090 cm^{-1}, 1030–1034 cm^{-1}, 960–961 cm^{-1}, 600–602 cm^{-1} and 561–562 cm^{-1} (Fig. 6, spectrum: SCL), corresponding to the peaks of HA (Fig. 7, spectrum: HA)[66,67], indicating the ability of MVs to produce HA. Addition of 1 mM or 2 mM P_i (corresponding, respectively, to a total P_i concentration of 2.42 mM or 3.42 mM in SCL) into the mineralization medium reduced the lag period of mineral formation induced by MVs from 3.5–4 h to 1.5–2 h or to 0.5 h, respectively (Fig. 5). In both cases, the minerals formed by MVs were identified as crystalline HA (Fig. 6, spectrum: P_i). Addition of 1 mM AMP reduced the induction phase from 3.5–4 h to 2.5–3 h (Fig. 5), i.e., to a lower extent as compared with the addition of 1 mM P_i, due to the time required for hydrolysis of AMP by TNAP. The mineral formed was also HA (Fig. 6, spectrum: AMP). However, addition of 0.33 mM ATP, increased the time delay of mineral formation from 3.5–4 h to 18–20 h (Fig. 5). This retardation was due to the inhibitory effect of ATP on HA deposition[68] or the formation of PP_i, a potent inhibitor of calcium–phosphate deposition[41–43]. The mineral phase produced by MVs in the presence of 0.33 mM ATP revealed HA and a small amount of other minerals, as suggested by the presence of a broad contour in the 1200–1000 cm^{-1} region (Fig. 6, spectrum: ATP), and as reported elsewhere[37].

THE REGULATORY EFFECT OF PP_i ON BIOMINERALIZATION

To identify the conditions to produce HA or other minerals, MVs were incubated in the SCL buffer with 2 mM Ca^{2+}, P_i at 1.42–3.42 mM concentration range and PP_i at 0.01–2.41 mM concentration range. P_i/PP_i ratio was calculated initially and during the induction phase of mineralization since PP_i was continuously hydrolyzed and both P_i and PP_i were involved in the mineral formation. The final P_i/PP_i ratio was determined for each initial P_i/PP_i ratio. The initial P_i/PP_i ratio (within 1.42–3.42 mM P_i and 0.01–2.41 mM PP_i) predetermined the type of mineral formed by MVs. Without PP_i, the period of induction phase was about 3 h when MVs were incubated in the SCL buffer with 2 mM Ca^{2+} [Fig. 8(A)], and 0.5 h when the SCL buffer was supplemented by 2 mM Ca^{2+} and 2 mM P_i corresponding to a total amount of 3.42 mM P_i in SCL [Fig. 8(B)]. A higher amount of P_i decreased the induction time of mineral formation. MVs incubated in the presence of Ca^{2+} and P_i formed crystalline HA (Fig. 9, spectrum I). The induction

Table I

Preparation of MVs from femoral and tibial growth plate cartilages of 17-day-old chick embryos. Growth plate cartilages were digested by collagenase. Hypertrophic chondrocytes were obtained by a centrifugation at 600× g for 10 min, the second pellet by a centrifugation at 13,000× g for 20 min and MVs by a last centrifugation at 70,000× g for 60 min. PME activity is expressed as μmol of p-NPP hydrolyzed per minute, per mg of MV proteins at pH 10.4

	Digest	Hypertrophic chondrocytes	Second pellet	MVs	Last supernatant
Specific PME activity (units/mg)	2.1 ± 0.2	5.2 ± 0.8	5.7 ± 0.6	25.0 ± 3.4	0.3 ± 0.1
Percentage of total activity (%)	100	18.2 ± 2.7	34.4 ± 3.5	39.7 ± 3.6	11.1 ± 1.1
Enrichment	1	2.5	2.7	11.9	0.1

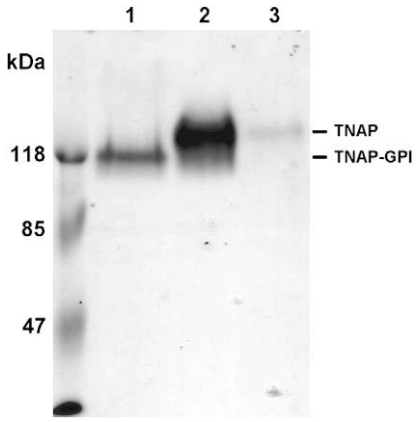

Fig. 3. BCIP–NBT visualization of TNAP in a 7.5% SDS-polyacrylamide gel. Lane 1, MVs; Lane 2, sMV (supernatant of MVs treated by PI-PLC); Lane 3, pMV.

time of mineralization increased from 3 to 6 h [Fig. 8(A)] after addition of 0.01 mM PP_i into the SCL medium with 2 mM Ca^{2+} (since SCL medium contained 1.42 mM P_i, the initial P_i/PP_i ratio was 142 ± 47 and final P_i/PP_i ratio was 198.3 ± 65.6, Table III). Addition of 0.024 mM PP_i and 2 mM P_i in SCL (total P_i was 3.42 mM in SCL medium; initial P_i/PP_i ratio was 142 ± 47 and final P_i/PP_i ratio was 198.3 ± 65.6), increased the induction time of mineralization from 0.5 to 2.5 h [Fig. 8(B)] and the mineral formed was crystalline HA (Fig. 9, spectrum II). At the initial P_i/PP_i ratio between infinite and 142 ± 47, the induction time increased (Table III), but the mineral formed was always HA (Table III). The turning point where the mineral phase contained a mixture of poorly crystalline HA and other minerals, was reached with an initial P_i/PP_i ratio of 71 ± 14.2 (Table III). The maximal induction time of mineral formation occurred upon addition of 0.05 ± 0.01 mM PP_i in SCL with 1.42 mM total P_i concentration [18 h, Fig. 8(A)] or 0.12 mM PP_i in SCL with 3.42 mM total P_i concentration [10 h, Fig. 8(B)], corresponding for both to an initial P_i/PP_i ratio of 28.4 ± 5.7 [Fig. 8(C)] and to a final P_i/PP_i ratio of 102.9 ± 20.7 (Table III). The minerals formed under these conditions were not HA as evidenced by the absence of characteristic HA bands at 960–961 cm^{-1}, 600–601 cm^{-1} and 560–562 cm^{-1}. Amorphous mixtures were produced (Fig. 9, spectrum III). The induction time of mineral formation decreased with the diminution of initial P_i/PP_i ratio from 28.4 ± 5.7, indicating faster mineral formation. Addition

Table II

Hydrolysis of p-NPP *and* PP_i *by MVs, the supernatant fraction (sMV) and the pellet fraction (pMV) of MVs treated by PI-PLC. PME activity was measured by hydrolysis of* p-NPP *at pH 10.4 ($PME_{10.4}$) and at pH 7.4 ($PME_{7.4}$). Pyrophosphatase activity was determined by hydrolysis of PP_i at pH 8.8 ($PP_{i8.8}$) and at pH 7.4 ($PP_{i7.4}$). The activities of MVs are expressed as μmol of substrate hydrolyzed per minute, per mg of MV proteins, under described conditions. The activities of sMV and pMV are expressed as percentages of total MV activities*

	MVs (units/mg)	% of total MV activity	
		sMV	pMV
$PME_{10.4}$	25.0 ± 3.40	92.0 ± 3.7	9.8 ± 0.9
$PME_{7.4}$	0.62 ± 0.10	91.0 ± 3.0	12.0 ± 1.0
$PP_{i8.8}$	3.70 ± 0.31	95.2 ± 2.8	6.0 ± 1.0
$PP_{i7.4}$	1.00 ± 0.09	96.0 ± 1.7	5.2 ± 0.8

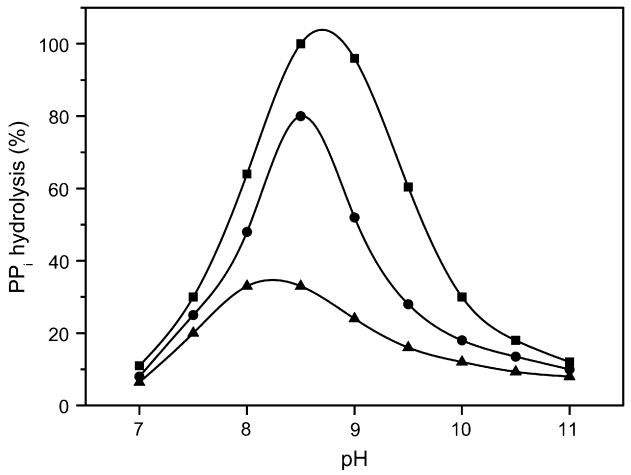

Fig. 4. The effect of pH on the PP_i hydrolysis by MVs. The pyrophosphatase activity of MVs was measured at different pH from 7 to 11, in the presence of different concentrations of PP_i: (■) 2 mM, (●) 1 mM, and (▲) 0.5 mM.

of 0.1 mM PP_i in SCL with 1.42 mM total P_i concentration (initial P_i/PP_i ratio of 14.2 ± 1.4 and final P_i/PP_i ratio of 24.5 ± 2.4) reduced the induction time of mineral formation to 9 h. It was further reduced to 7 h with the addition of 0.5 mM PP_i (initial P_i/PP_i ratio of 2.8 ± 0.3 and final ratio of 6.2 ± 0.7) and to 5 h with 1 mM PP_i (initial P_i/PP_i ratio of 1.4 ± 0.1 and final ratio of 2.8 ± 0.3) [Fig. 8(A)]. We observed also a decrease of induction time of mineral formation at the same P_i/PP_i ratio but with higher PP_i concentrations in SCL medium containing 3.42 mM P_i [Fig. 8(B)]. Due to the higher amount of PP_i and P_i, there was a higher amount of mineral formed as evidenced by the larger turbidity and the kinetics [Fig. 8(B) vs Fig. 8(A)]. Although the mineral formation in MVs was stimulated with higher concentrations of PP_i, the nature of mineral deposits was different. At the initial P_i/PP_i ratios between 14.2 ± 1.4 and 2.8 ± 0.3, the mineral phase was composed of a mixture

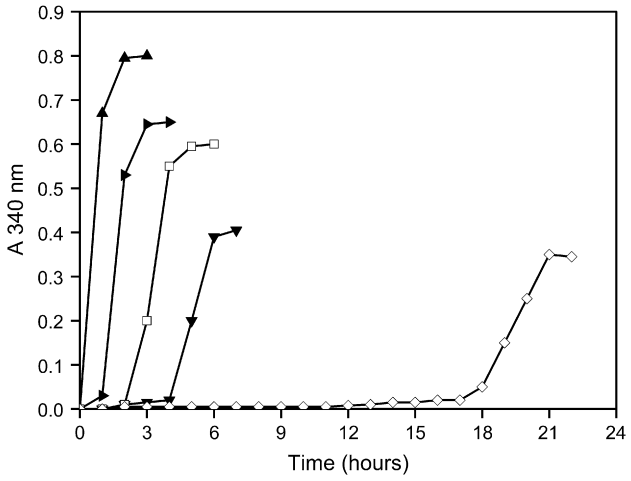

Fig. 5. Kinetics of mineral formation by MVs. MVs were incubated at 37°C in SCL buffer containing 2 mM Ca^{2+} and 1.42 mM P_i with additional P_i or phosphate substrates, as follows: (▼) without additional substrates, (►) total $P_i = 2.42$ mM, (▲) total $P_i = 3.42$ mM, (□) 1 mM AMP, and (◇) 0.33 ATP. Mineral formation was assessed by light scattering at 340 nm.

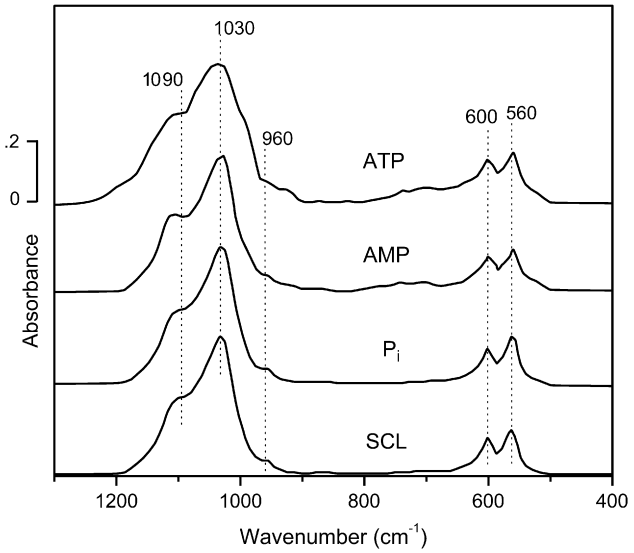

Fig. 6. Infrared spectra of minerals formed by MVs in the presence of different concentrations of P_i or different phosphate substrates. MVs were incubated at 37°C in SCL buffer containing 2 mM Ca^{2+} and 1.42 mM P_i with additional P_i or phosphate substrates: without additional substrates as a control (spectrum SCL), total $P_i = 3.42$ mM (spectrum P_i), 1 mM AMP (spectrum AMP), 0.33 ATP (spectrum ATP).

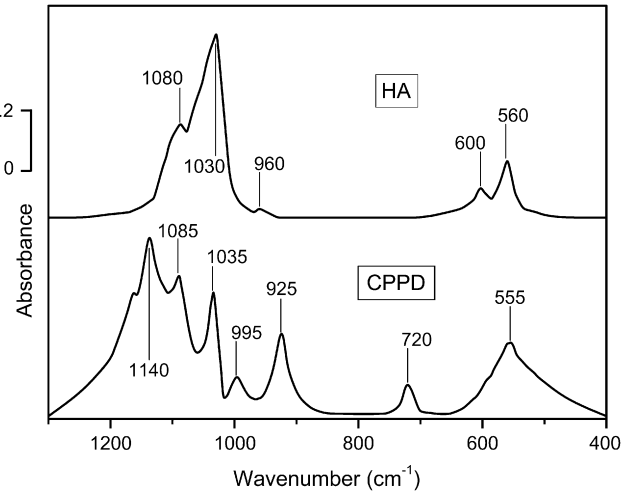

Fig. 7. Infrared spectra of HA and CPPD standards.

of minerals, including CPPD (Fig. 9, spectrum IV), as characterized by the appearance of the characteristic CPPD bands at 1140 cm^{-1}, 925 cm^{-1}, 725 cm^{-1} and 555 cm^{-1} (Fig. 7, spectrum: CPPD). At the initial P_i/PP_i ratio lower than 2.8 ± 0.3, the spectrum of the mineral formed by MVs resembled to CPPD (Fig. 9, spectrum V). CPPD mineral was exclusively produced by MVs when the initial P_i/PP_i ratio was lower than 1.4 ± 0.1 (Fig. 9, spectrum VI).

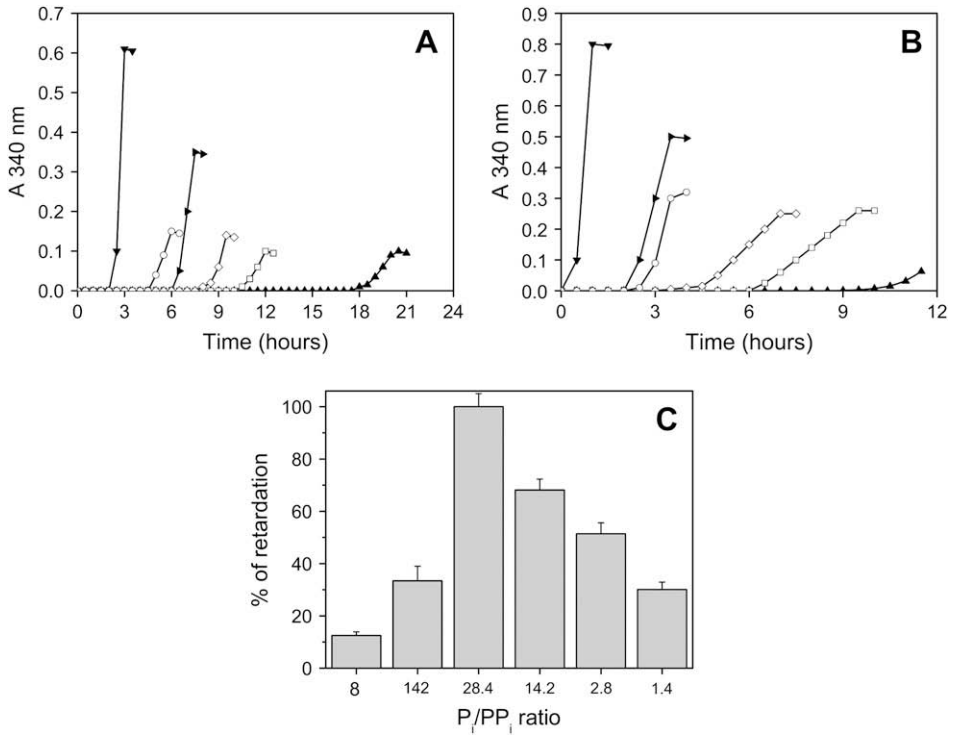

Fig. 8. Retardation of PP_i-initiated mineral formation. (A) MVs were incubated at 37°C in SCL buffer containing 2 mM Ca^{2+}, 1.42 mM P_i and PP_i at various concentrations: (▼) without additional PP_i, (►) 0.01 mM, (▲) 0.05 mM, (□) 0.1 mM, (◇) 0.5 mM and (○) 1 mM PP_i corresponding to an initial P_i/PP_i ratio of 142, 28.4, 14.2, 2.8, and 1.4, respectively. (B) MVs were incubated at 37°C in SCL buffer containing 2 mM Ca^{2+}, 3.42 mM P_i and different concentrations of PP_i: (▼) without additional PP_i, (►) 0.024 mM, (▲) 0.12 mM, (□) 0.24 mM, (◇) 1.2 mM and (○) 2.41 mM PP_i, corresponding to the same P_i/PP_i ratio as in panel A. (C) All results were combined and normalized as percentages of the maximal retardation of mineralization induced by PP_i.

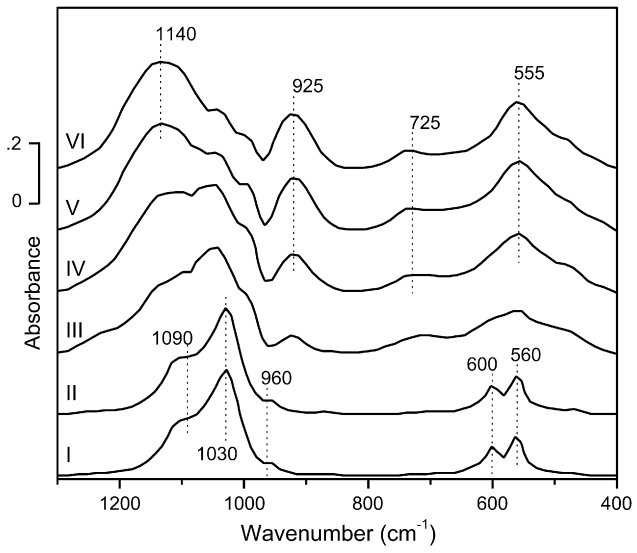

Fig. 9. Infrared spectra of minerals produced by MVs at different P_i/PP_i molar ratios: (I) no PP_i, (II) 142, (III) 28.4, (IV) 14.2, (V) 2.8 and (VI) 1.4. MVs were incubated at 37°C in SCL buffer containing 2 mM Ca^{2+}, 3.42 mM P_i and PP_i at 0, 0.024 mM, 0.12 mM, 0.24 mM, 1.2 mM or 2.41 mM.

Under the same conditions, no CPPD was formed in SCL medium without MVs.

Discussion

Our report focused on the conditions favoring HA and CPPD minerals induced by MVs from growth plate cartilage. MVs were used to mimic pathological calcification, since the initiation of mineral formation mediated by MVs during endochondral calcification is similar to that which appears in a variety of pathologic calcification[6]. Although MV model has the disadvantage that matrix and cellular issues cannot be addressed, it provides an easily quantifiable and well-characterized model to analyze the initiation of HA or CPPD formation[47]. MVs served to model arthritic crystal deposition characterized by HA or CPPD deposits in joint cartilage. In the absence of inhibitors, Ca^{2+}/P_i ratio and the $Ca^{2+} \times P_i$ product are critical factors affecting the kinetics of the biomineralization process[69]. Increasing the P_i concentration (Fig. 5) and addition of phosphomonoester substrates of TNAP, such as AMP, reduced the induction time of HA formation (Fig. 5). However, addition of ATP, another source of P_i after its hydrolysis, led to a high retardation of the induction phase of mineralization (Fig. 5) and to a mixture of poorly crystalline HA and other minerals (Fig. 3, spectrum: ATP), consistent with Zhang *et al.*[39]. The retardation was due to the inhibitory effect of ATP[68] or PP_i[41–43], on the HA formation. ATP is a source of P_i (after its hydrolysis by TNAP, ATPases and other PME enzymes) but also a source of PP_i after its hydrolysis by NPP1 and TNAP[39]. PP_i, when hydrolyzed, provides P_i for HA formation but inhibits the seeding of calcium–phosphate minerals itself. In addition, high concentrations of PP_i led to the precipitation of immature CPPD mineral. Alternatively, metastable equilibrium between Ca^{2+}, P_i and PP_i can be disturbed, inducing mineral formations without MVs. Cheng and Pritzker[70] reported that HA was formed in aqueous solution when P_i/PP_i was higher than 100, while CPPD was produced when P_i/PP_i was less than 3. MVs from growth plate cartilages are able to produce CPPD minerals[37,71]. Since osteoarthritic MVs and growth plate MVs own similar protein machinery associated with mineralization, these findings underline a mechanism of CPPD pathological deposit. Our data emphasize that not only PP_i concentration affected the nature of the formed mineral but also the P_i/PP_i ratio is a key parameter to favor HA or CPPD formation as proposed previously[37]. The P_i/PP_i ratio is a determinant factor leading to pathological mineralization or its inhibition. Initial P_i/PP_i ratio higher than 140 led to HA deposition, mimicking conditions during endochondral bone formation or arthritic crystal deposition. When P_i/PP_i ratio was lower than 70, it inhibited the MV-induced seeding of HA, which corresponds to the conditions where mineralization is inhibited. An initial P_i/PP_i ratio lower than 2.8 led to deposits of pathological CPPD, while initial P_i/PP_i ratio higher than 28.4 inhibited CPPD formation. The P_i/PP_i ratio could reflect somehow the overall differentiation states of chondrocytes (mature vs hypertrophic), the levels of expression of TNAP, NPP1 or other proteins affecting P_i and PP_i concentrations as well as the balance between pro- and anti-calcification factors and may serve as an indicator of calcification process.

Table III

The effect of the P_i/PP_i ratio on the mineralization mediated by MVs. MVs were incubated in the SCL buffer containing 2 mM Ca^{2+}, P_i at 1.42–3.42 mM concentration range and PP_i at 0.01–2.41 mM concentration range. Initial P_i/PP_i ratios and P_i/PP_i ratios prior to the onset of calcification were calculated. The kinetics of mineralization was followed by light scattering at 340 nm and the minerals formed by MVs were identified by infrared spectroscopy (the numbering of spectra corresponded to the infrared spectra in Fig. 9 and to the minerals formed at a specific P_i/PP_i ratio as indicated in the table). Induction time was the longest (100%) at initial $[P_i]/[PP_i] = 28.4 \pm 5.7$ and the lowest (12.5 ± 1.4) in the absence of PP_i

Initial $[P_i]/[PP_i]$	Final $[P_i]/[PP_i]$	Induction time (%)	Minerals formed, IR spectra in Fig. 9
∞	∞	12.5 ± 1.4	HA, Spectrum I
142 ± 47	198.3 ± 65.6	33.4 ± 5.6	HA, Spectrum II
71 ± 14.2	138.7 ± 27.7	50.1 ± 3.5	HA + other
28.4 ± 5.7	102.9 ± 20.7	100 ± 5.0	CPPD + other, Spectrum III
14.2 ± 1.4	24.5 ± 2.4	68.1 ± 4.2	CPPD + other, Spectrum IV
2.8 ± 0.3	6.2 ± 0.7	51.4 ± 4.2	CPPD, Spectrum V
1.4 ± 0.1	2.8 ± 0.3	30.1 ± 2.8	CPPD, Spectrum VI

Conflict of interest

None of the authors of this paper have any financial and personal relationships with people or organization that could inappropriately influence (bias) their work.

Acknowledgments

We thank Dr Laurence Bessuelle for her help with electron microscopy and Dr John Carew for correcting the English. This work was supported by a Polonium grant (05819NF), CNRS (France) and by a grant N301 025 32-1120 from Polish Ministry of Science and Higher Education.

References

1. Thouverey C, Bleicher F, Bandorowicz-Pikula J. Extracellular ATP and its effects on physiological and pathological mineralization. Curr Opin Orthop 2007;18:460–6.
2. Balcerzak M, Hamade E, Zhang L, Pikula S, Azzar G, Radisson J, *et al*. The roles of annexins and alkaline phosphatase in mineralization process. Acta Biochim Pol 2003;50:1019–38.
3. Kirsch T. Determinants of pathological mineralization. Curr Opin Rheumatol 2006;18:174–80.
4. Van de Lest CHA, Vaandrager AB. Mechanisms of cell-mediated mineralization. Curr Opin Orthop 2007;18:434–43.
5. Kirsch T. Physiological and pathological mineralization: a complex multifactorial process. Curr Opin Orthop 2007;18:425–7.
6. Anderson HC. The role of matrix vesicles in physiological and pathological calcification. Curr Opin Orthop 2007;18:428–33.
7. Karpouzas GA, Terkeltaub RA. New developments in the pathogenesis of articular cartilage calcification. Curr Rheumatol Rep 1999;1:121–7.
8. Derfus BA, Kurtin SM, Camacho NP, Kurup I, Ryan LM. Comparison of matrix vesicles derived from normal and osteoarthritic human articular cartilage. Connect Tissue Res 1996;35:337–42.
9. Derfus B, Kranendonk S, Camacho N, Mandel N, Kushnaryov V, Lynch K, *et al*. Human osteoarthritic cartilage matrix vesicles generate both calcium pyrophosphate dihydrate and apatite *in vitro*. Calcif Tissue Int 1998;63:258–62.
10. Anderson HC. Calcific diseases: a concept. Arch Pathol Lab Med 1983; 107:341–8.
11. Reginato AM, Shapiro IM, Lash JW, Jimenez SA. Type X collagen alterations in rachitic chick epiphyseal growth cartilage. J Biol Chem 1988; 263:9938–45.
12. Hatori M, Klatte KJ, Teixeira CC, Shapiro IM. End labeling studies of fragmented DNA in the avian growth plate: evidence of apoptosis in terminally differentiated chondrocytes. J Bone Miner Res 1995;10: 1960–8.
13. Binette F, McQuaid DP, Haudenschild DR, Yaeger PC, McPherson JM, Tubo R. Expression of a stable articular cartilage phenotype without evidence of hypertrophy by adult human articular chondrocytes *in vitro*. J Orthop Res 1998;16:207–16.
14. Kirsch T, Nah HD, Shapiro IM, Pacifici M. Regulated production of mineralization-competent matrix vesicles in hypertrophic chondrocytes. J Cell Biol 1997;137:1149–60.
15. Anderson HC. Molecular biology of matrix vesicles. Clin Orthop Relat Res 1995;266–80.
16. Anderson HC, Garimella R, Tague SE. The role of matrix vesicles in growth plate development and biomineralization. Front Biosci 2005; 10:822–37.
17. Ali SY. Analysis of matrix vesicles and their role in the calcification of epiphyseal cartilage. Fed Proc 1976;35:135–42.
18. Paulsen F, Tillmann B. Composition of the extracellular matrix in human cricoarytenoid joint articular cartilage. Arch Histol Cytol 1999;62: 149–63.
19. Sweet MB, Thonar EJ, Immelman AR, Solomon L. Biochemical changes in progressive osteoarthrosis. Ann Rheum Dis 1977;36:387–98.
20. Pritzker KP. Crystal-associated arthropathies: what's new in old joints. J Am Geriatr Soc 1980;28:439–45.
21. Ali SY. Apatite-type crystal deposition in arthritic cartilage. Scan Electron Microsc 1985;4:1555–66.
22. Anderson HC. Mechanisms of pathologic calcification. Rheum Dis Clin North Am 1988;14:303–19.
23. Anderson HC. Matrix vesicles and calcification. Curr Rheumatol Rep 2003;5:222–6.
24. Cheung HS, Kurup IV, Sallis JD, Ryan LM. Inhibition of calcium pyrophosphate dihydrate crystal formation in articular cartilage vesicles and cartilage by phosphocitrate. J Biol Chem 1996;271:28082–5.
25. Derfus BA, Camacho NP, Olmez U, Kushnaryov VM, Westfall PR, Ryan LM, *et al*. Transforming growth factor beta-1 stimulates articular chondrocyte elaboration of matrix vesicles capable of greater calcium pyrophosphate precipitation. Osteoarthritis Cartilage 2001;9: 189–94.
26. Kirsch T, Swoboda B, Nah HD. Activation of annexin II and V expression, terminal differentiation, mineralization and apoptosis in human osteoarthritic cartilage. Osteoarthritis Cartilage 2000;8:294–302.
27. Rees JA, Ali SY. Ultrastructural localisation of alkaline phosphatase activity in osteoarthritic human articular cartilage. Ann Rheum Dis 1988;47:747–53.
28. Einhorn TA, Gordon SL, Siegel SA, Hummel CF, Avitable MJ, Carty RP. Matrix vesicle enzymes in human osteoarthritis. J Orthop Res 1985;3: 160–9.
29. Johnson K, Hashimoto S, Lotz M, Pritzker K, Goding J, Terkeltaub R. Up-regulated expression of the phosphodiesterase nucleotide pyrophosphatase family member PC-1 is a marker and pathogenic factor for knee meniscal cartilage matrix calcification. Arthritis Rheum 2001;44:1071–81.
30. Nanba Y, Nishida K, Yoshikawa T, Sato T, Inoue H, Kuboki Y. Expression of osteonectin in articular cartilage of osteoarthritic knees. Acta Med Okayama 1997;51:239.
31. Nakase T, Miyaji T, Tomita T, Kaneko M, Kuriyama K, Myoui A, *et al*. Localization of bone morphogenetic protein-2 in human osteoarthritic cartilage and osteophyte. Osteoarthritis Cartilage 2003;11:278–84.
32. Wang X, Manner PA, Horner A, Shum L, Tuan RS, Nuckolls GH. Regulation of MMP-13 expression by RUNX2 and FGF2 in osteoarthritic cartilage. Osteoarthritis Cartilage 2004;12:963–73.
33. Johnson KA, Hessle L, Vaingankar S, Wennberg C, Mauro S, Narisawa S, *et al*. Osteoblast tissue-nonspecific alkaline phosphatase antagonizes and regulates PC-1. Am J Physiol Regul Integr Comp Physiol 2000;279:R1365–77.
34. Anderson HC, Harmey D, Camacho NP, Garimella R, Sipe JB, Tague S, *et al*. Sustained osteomalacia of long bones despite major improvement in other hypophosphatasia-related mineral deficits in tissue nonspecific alkaline phosphatase/nucleotide pyrophosphatase phosphodiesterase 1 double-deficient mice. Am J Pathol 2005;166: 1711–20.
35. Hessle L, Johnson KA, Anderson HC, Narisawa S, Sali A, Goding JW, *et al*. Tissue-nonspecific alkaline phosphatase and plasma cell membrane glycoprotein-1 are central antagonistic regulators of bone mineralization. Proc Natl Acad Sci U S A 2002;99:9445–9.
36. Golub EE, Boesze-Battaglia K. The role of alkaline phosphatase in mineralization. Curr Opin Orthop 2007;18:444–8.
37. Garimella R, Bi X, Anderson HC, Camacho NP. Nature of phosphate substrate as a major determinant of mineral type formed in matrix vesicle-mediated *in vitro* mineralization: an FTIR imaging study. Bone 2006;38:811–7.
38. Hamade E, Azzar G, Radisson J, Buchet R, Roux B. Chick embryo anchored alkaline phosphatase and mineralization process *in vitro*. Eur J Biochem 2003;270:2082–90.
39. Zhang L, Balcerzak M, Radisson J, Thouverey C, Pikula S, Azzar G, *et al*. Phosphodiesterase activity of alkaline phosphatase in ATP-initiated Ca^{2+} and phosphate deposition in isolated chicken matrix vesicles. J Biol Chem 2005;280:37289–96.
40. Blumenthal NC. Mechanisms of inhibition of calcification. Clin Orthop Relat Res 1989;279–89.
41. Register TC, Wuthier RE. Effect of pyrophosphate and two diphosphonates on 45Ca and $32P_i$ uptake and mineralization by matrix vesicle-enriched fractions and by hydroxyapatite. Bone 1985;6: 307–12.
42. Tanimura A, McGregor DH, Anderson HC. Matrix vesicles in arthrosclerotic calcification. Proc Soc Exp Biol Med 1983;172:173–7.
43. Tenenbaum HC. Levamisole and inorganic pyrophosphate inhibit beta-glycerophosphate induced mineralization of bone formed *in vitro*. Bone Miner 1987;3:13–26.
44. Terkeltaub RA. Inorganic pyrophosphate generation and disposition in pathophysiology. Am J Physiol Cell Physiol 2001;281:C1–C11.
45. Ryan LM, Rosenthal AK. Metabolism of extracellular pyrophosphate. Curr Opin Rheumatol 2003;15:311–4.
46. Viriyavejkul P, Wilairatana V, Tanavalee A, Jaovisidha K. Comparison of characteristics of patients with and without calcium pyrophosphate dihydrate crystal deposition disease who underwent total knee replacement surgery for osteoarthritis. Osteoarthritis Cartilage 2007; 15:232–5.
47. Gohr C. *In vitro* models of calcium crystal formation. Curr Opin Rheumatol 2004;16:263–7.
48. Harmey D, Hessle L, Narisawa S, Johnson KA, Terkeltaub R, Millan JL. Concerted regulation of inorganic pyrophosphate and osteopontin by akp2, enpp1, and ank: an integrated model of the pathogenesis of mineralization disorders. Am J Pathol 2004;164:1199–209.
49. Ho AM, Johnson MD, Kingsley DM. Role of the mouse *ank* gene in control of tissue calcification and arthritis. Science 2000;289:265–70.
50. Zaka R, Williams CJ. Role of the progressive ankylosis gene in cartilage mineralization. Curr Opin Rheumatol 2006;18:181–6.
51. Johnson K, Terkeltaub R. Upregulated ank expression in osteoarthritis can promote both chondrocyte MMP-13 expression and calcification *via* chondrocyte extracellular PP_i excess. Osteoarthritis Cartilage 2004;12:321–35.
52. Johnson K, Terkeltaub R. Inorganic pyrophosphate (PP_i) in pathologic calcification of articular cartilage. Front Biosci 2005;10:988–97.
53. Hirose J, Ryan LM, Masuda I. Up-regulated expression of cartilage intermediate-layer protein and ANK in articular hyaline cartilage from patients with calcium pyrophosphate dihydrate crystal deposition disease. Arthritis Rheum 2002;46:3218–29.
54. Wu LN, Yoshimori T, Genge BR, Sauer GR, Kirsch T, Ishikawa Y, *et al*. Characterization of the nucleational core complex responsible for mineral induction by growth plate cartilage matrix vesicles. J Biol Chem 1993;268:25084–94.
55. Balcerzak M, Radisson J, Azzar G, Farlay D, Boivin G, Pikula S, *et al*. A comparative analysis of strategies for isolation of matrix vesicles. Anal Biochem 2007;361:176–82.

56. Laemmli UK. Cleavage of structural proteins during the assembly of the head of bacteriophage T4. Nature 1970;227:680–5.
57. Towbin H, Staehelin T, Gordon J. Electrophoretic transfer of proteins from polyacrylamide gels to nitrocellulose sheets: procedure and some applications. Proc Natl Acad Sci U S A 1979;76:4350–4.
58. Cyboron GW, Wuthier RE. Purification and initial characterization of intrinsic membrane-bound alkaline phosphatase from chicken epiphyseal cartilage. J Biol Chem 1981;256:7262–8.
59. Wu LN, Genge BR, Dunkelberger DG, LeGeros RZ, Concannon B, Wuthier RE. Physicochemical characterization of the nucleational core of matrix vesicles. J Biol Chem 1997;272:4404–11.
60. Wu LN, Sauer GR, Genge BR, Valhmu WB, Wuthier RE. Effects of analogues of inorganic phosphate and sodium ion on mineralization of matrix vesicles isolated from growth plate cartilage of normal rapidly growing chickens. J Inorg Biochem 2003;94:221–35.
61. Anderson HC, Cecil R, Sajdera SW. Calcification of rachitic rat cartilage *in vitro* by extracellular matrix vesicles. Am J Pathol 1975;79:237–54.
62. Majeska RJ, Wuthier RE. Studies on matrix vesicles isolated from chick epiphyseal cartilage: association of pyrophosphatase and ATPase activities with alkaline phosphatase. Biochim Biophys Acta 1975;391:51–60.
63. Robison R. The possible significance of hexosephosphoric esters in ossification. Biochem J 1923;17:286–93.
64. McLean FM, Keller PJ, Genge BR, Walters SA, Wuthier RE. Disposition of preformed mineral in matrix vesicles. Internal localization and association with alkaline phosphatase. J Biol Chem 1987;262: 10481–8.
65. Whyte MP. Hypophosphatasia and the role of alkaline phosphatase in skeletal mineralization. Endocr Rev 1994;15:439–61.
66. Pleshko N, Boskey A, Mendelsohn R. Novel infrared spectroscopic method for the determination of crystallinity of hydroxyapatite minerals. Biophys J 1991;60:786–93.
67. Sauer GR, Wuthier RE. Fourier transform infrared characterization of mineral phases formed during induction of mineralization by collagenase-released matrix vesicles *in vitro*. J Biol Chem 1988;263: 13718–24.
68. Boskey AL, Boyan BD, Schwartz Z. Matrix vesicles promote mineralization in a gelatin gel. Calcif Tissue Int 1997;60:309–15.
69. Walhmu WB, Wu LN, Wuthier RE. Effects of Ca/P_i ratio, $Ca^{2+} \times P_i$ ion product, and pH of incubation fluid on accumulation of $45Ca^{2+}$ by matrix vesicles *in vitro*. Bone Miner 1990;8:195–209.
70. Cheng PT, Pritzker KP. Pyrophosphate, phosphate ion interaction: effects on calcium pyrophosphate and calcium hydroxyapatite crystal formation in aqueous solutions. J Rheumatol 1983;10:769–77.
71. Hsu HH, Camacho NP, Anderson HC. Further characterization of ATP-initiated calcification by matrix vesicles isolated from rachitic rat cartilage. Membrane perturbation by detergents and deposition of calcium pyrophosphate by rachitic matrix vesicles. Biochim Biophys Acta 1999;1416:320–32.